Available online at www.sciencedirect.com
ScienceDirect
Trans. Nonferrous Met. Soc. China 33(2023) 2879−2897
Transactions of Nonferrous Metals Society of China
www.tnmsc.cn

Effect of deep cryogenic cycling treatment on structure and properties of metallic glass: A review

Ming-zi WANG[1], Wei GUO[1,2,3], Shu-lin LÜ[1], Shu-sen WU[1]

1. State Key Laboratory of Materials Processing and Die & Mould Technology, School of Materials Science and Engineering, Huazhong University of Science and Technology, Wuhan 430074, China;
2. State Key Laboratory of Advanced Design and Manufacturing for Vehicle Body, Hunan University, Changsha 410082, China;
3. Research Institute of Huazhong University of Science and Technology in Shenzhen, Shenzhen 518057, China

Received 18 May 2022; accepted 21 September 2022

Abstract: Recent researches have shown that metallic glasses (MGs) can be rejuvenated to a more metastable energy state by thermal or mechanical approaches, which causes a looser atomic packing. This process can effectively improve the overall plasticity of MGs. The present work started with the concept of ageing and rejuvenation of MGs, briefly introducing the probable methods to rejuvenate the MGs, then the advantages and disadvantages of various methods were summarized, and the effects of deep cryogenic cycling method (a non-destructive method to sample morphology and feasible to conduct) were investigated in detail. The effects of treating parameters on the degree of rejuvenation and the effects of rejuvenation on the mechanical and magnetic properties of MGs were also summarized. Finally, some conclusions in this field are drawn and some important questions that deserve further study are put forward.
Key words: metallic glass; rejuvenation; deep cryogenic cycling; relaxation enthalpy; plasticity

1 Introduction

Metallic glasses (MGs) [1−3] are fabricated by sufficiently rapid cooling from liquid state to avoid crystallization and maintain a disordered structure in solid state [4]. They have attracted research interests because of their excellent properties, such as high strength [5], large elastic limit [6] and high corrosion resistance [7]. Due to the rapid quenching process, MGs possess a metastable structure, which indicates that at a certain temperature and time, MGs will spontaneously relax to a lower or a more stable energy state, accompanied by a rearrangement of local atoms and a reduction of structural inhomogeneities, known as ageing or relaxation process [8−10]. In practical applications, ageing is inevitable, altering the internal structure and deteriorating the properties. Normally, aged metallic glasses exhibit brittle fracture accompanied by free volume annihilation [8,11], and thus ageing limits the widespread application of metallic glasses.

In recent years, rejuvenation process [12−14], an opposite process of ageing, could tailor the MGs to an even higher energy state without forming any crystalline phase in the microstructure, i.e., tending to a more metastable state or a more desirable amorphous structure [8,15]. Figure 1 shows the schematic of ageing and rejuvenation processes and their correlation based on potential energy landscapes (PEL) and 2D schematic of atomic motion. The rejuvenated metallic glasses exhibit better properties, such as higher plasticity [17]. Thus,

Corresponding author: Wei GUO, Tel: +86-27-87556262, E-mail: weiguo@hust.edu.cn
DOI: 10.1016/S1003-6326(23)66305-8

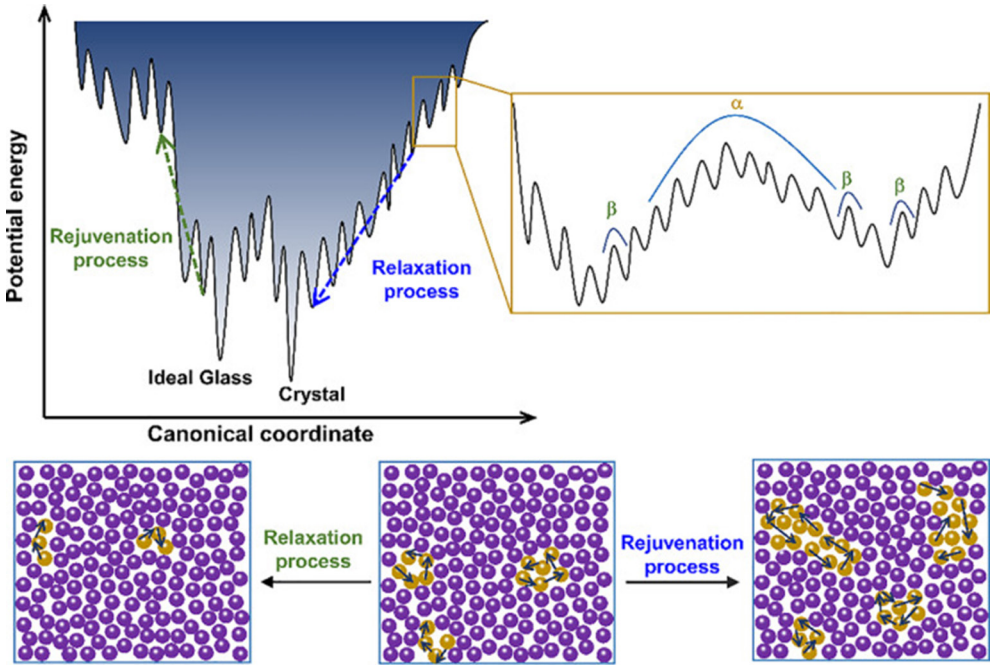

Fig. 1 Schematic of rejuvenation process, relaxation process, β relaxation and α relaxation as well as their correlation: 1D schematic of corresponding potential energy landscapes (top panel); 2D schematic of atomic motion (bottom panel) (The purple and golden balls represent elastic matrix and high mobility atoms, respectively, and the black arrows indicate possible movements of atoms) [16]

the rejuvenation can further expand the application of MGs. Meanwhile, the research [18] on the structural evolution and mechanism of rejuvenation is also beneficial to a deeper understanding of the disordered structures themselves. At present, the main methods to rejuvenate the MGs are divided into mechanical method [19,20], thermo-mechanical method [21,22] and thermal method [23,24].

The mechanical treatment [11,25−27] directly applies the load to the metallic glass to transit the structure to a more disordered state driven by the external work. Elastostatic loading [28] is one of the commonly-used mechanical methods, which loads a metallic glass under a stress below the yield strength for a long period of time. The irreversible non-affine deformation occurs slowly and the sample is rejuvenated. LOUZGUINE-LUZGIN et al [29] developed method of cyclic compression within the elastic loading and achieved the structural rejuvenation of $Zr_{61}Cu_{27}Fe_2Al_{10}$ metallic glass. The overall elastic modulus increases by ~0.8% due to the anelasticity, which also reflected that the cyclic loading appears to accelerate the development of anelastic strain. The outstanding advantage of this treatment is that it can achieve uniform rejuvenated structures on a macroscopic scale, but the limitation of this treatment is the long time scale to achieve rejuvenation. Recently, a novel treatment method is proposed to achieve a high degree of structural rejuvenation in a short time by applying a large stress. It can rejuvenate Zr-based MGs in about 365 ns based on a two-target plate impact technique as shown in Fig. 2. This work improves the time scale for rejuvenation of metallic glass structures by at least 10 orders of magnitude, expanding the applications of such materials and deepening the knowledge of ultrafast dynamics of glasses.

However, the degree of rejuvenation during such treatment is usually low, and thus the server plastic deformation, such as cold rolling [31], shot-peening [32,33] and high-pressure torsion (HPT) [34−36], have been introduced to improve the rejuvenation degree. MENG et al [37] found that the rejuvenated region is preferentially transformed into a shear deformation zone during high-pressure torsion, as shown in Fig. 3, which indicates that the a higher rotation number induces a higher structural relaxation enthalpy. HPT deformation significantly reduces the extent of strain localization and the rejuvenated sample tends

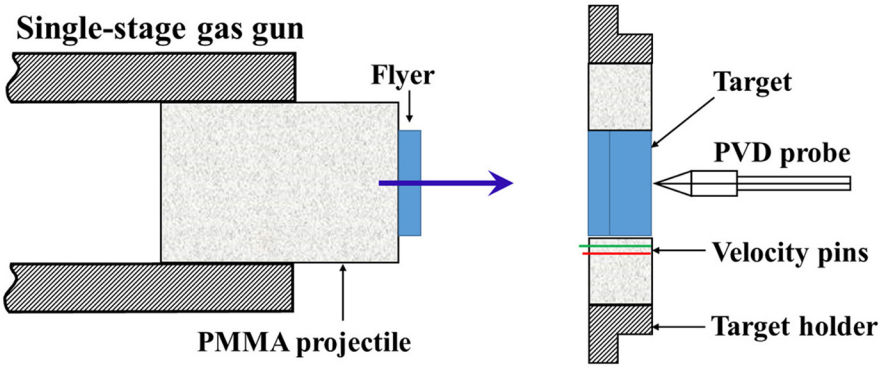

Fig. 2 Schematic of light-gas gun-driven plate impact experimental configuration [30]

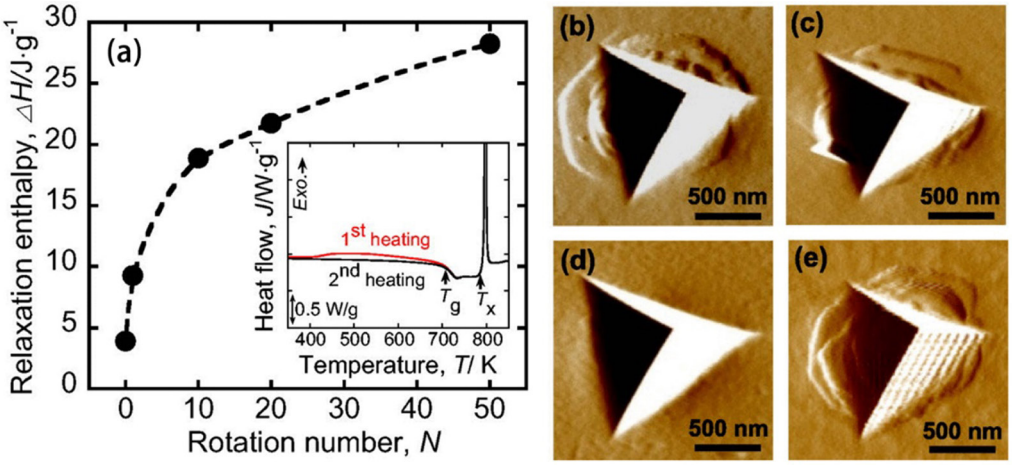

Fig. 3 Calculated structural relaxation enthalpy as function of rotation number (The inset shows DSC curves of the sample with N=50, and the red and black lines denote the 1st and 2nd heating curves, respectively) (a); Scanning probe microscope (SPM) images of indents in as-cast state (b) and HPT deformed samples with N=10 (c), N=50 (d) and N=50 (e) after annealing at 673 K for 1 h [37]

to possess more homogeneous plastic deformation. In addition, once the rejuvenated sample was annealed after HPT, the degree of rejuvenation decreases and the elastic modulus and hardness also improve. The structure during high-pressure torsion varies from the edge to the center of the sample because of different strains.

LI et al [38] used $Cu_{50}Zr_{50}$ MG models to perform cyclic loading via simulation, and the rejuvenation process upon cyclic elastic loading is confirmed by characterizing tensile deformation behaviors, as shown in Fig. 4. Different tensile deformation behaviors could be found in three simulated models (see Fig. 4(a)), which suggests that cyclic loading within the elastic regime can effectively modify the mechanical properties. Furthermore, for the $CuZr_{0\text{-cycle}}$ sample, a significant stress drop occurs after reaching the peak stress, corresponding to a rapid shear localization within a single dominant shear band, as shown in the corresponding snapshot for Sample 1 in Fig. 4(b). Meanwhile, $CuZr_{10\text{-cycle}}$ shows a similar stress drop, but in relatively smaller magnitude. $CuZr_{50\text{-cycle}}$ sample shows almost perfect plastic flow, and no localized shear band behavior is observed even at the maximum strain applied (see Sample 4 in Fig. 4(b)). Overall, a higher cycling loading numbers lead to a more pronounced rejuvenation.

Large deformations based on mechanical methods can easily lead to the formation of nanoscale shear bands in metallic glasses. Although the shear zone itself has a high degree of rejuvenation, its highly spatial localization greatly reduces the overall rejuvenation of the sample, thus limiting the further application of metallic glasses. In addition, mechanical process is usually limited by the loading apparatus, and the change in sample morphology is irreversible.

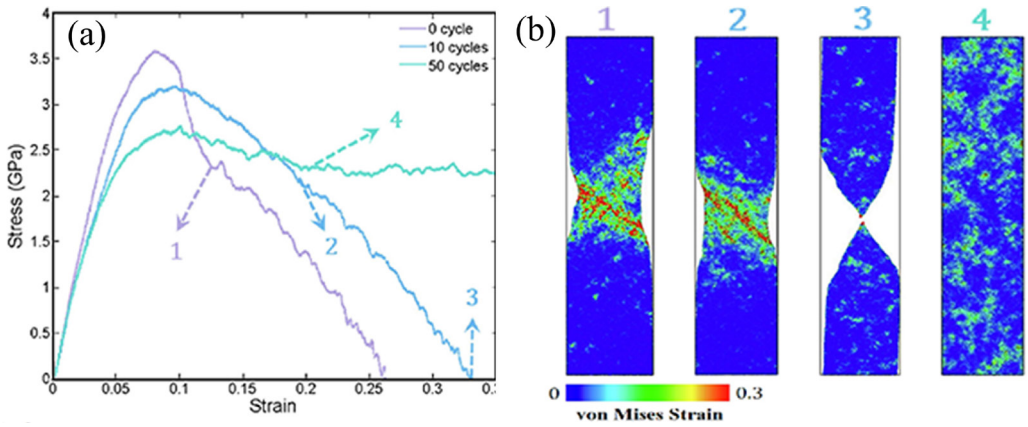

Fig. 4 Stress−strain curves of simulated $CuZr_{0\text{-cycle}}$, $CuZr_{10\text{-cycle}}$ and $CuZr_{50\text{-cycle}}$ samples (a); Snapshots of spatial distributions of elastic atoms colored by the von Mises strain corresponded to selected points for 3 models (b) [38]

Compared to mechanical methods, thermal treatment is non-destructive and avoids the shape change. Moreover, unlike the applied elastic stress in mechanical treatment, the treating in thermal methods is isotropic and homogeneous. Thermal treatment can be applied to a variety of sample shapes (such as ribbons, rods or blocks) and can be repeated as needed. Meanwhile, the residual stress generated by thermal treatment is well below the elastic limit and barely induces the deformation. At present, there are two main thermal treatments: recovery annealing [14,15,39−41] and deep cryogenic cycling [13,42]. In the present work, the existing research on deep cryogenic cycling is summarized in detail. Firstly, the researchers found that deep cryogenic treatment, placing the sample in liquid nitrogen and holding it for a period of time, could improve the plasticity of the sample without degrading its hardness. The followed-up study found that the properties can be even improved by further cycling process. Deep cryogenic cycling treatment refers to a cycling between a lower limit temperature (e.g., liquid nitrogen, 77 K) and a certain higher temperature (e.g., ambient temperature).

As shown in Fig. 5, the main parameter during deep cryogenic cycling treatment is the temperature range (maximum and minimum temperature, T_a and T_b), holding time at both low and high temperatures (t_a and t_b), number of cycles (N), etc. Other factors that affect the rejuvenation process includes the initial relaxation state and the composition. We will summarize these parameter effects on the rejuvenation process, as well as the relations between rejuvenation and properties.

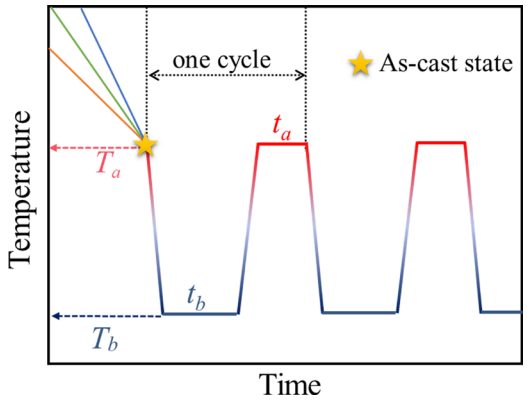

Fig. 5 Illustration of temperature change during deep cryogenic cycling process

The deep cryogenic cycling method applied in most researches is simply placing the sample in liquid nitrogen and holding for a certain time, and then reheating the sample to ambient temperature. The temperature cannot be precisely recorded during cycling and it is hard to carry out automatically. GUO et al [42] developed an experimental instrument for deep cryogenic cycling (DCT) treatment. As shown in Fig. 6, the stage is connected to a liquid nitrogen flow pipe and it can be cooled down to and held at 77 K. The sample is fixed in a copper sample-holder and contacted with a thermocouple to record the sample temperature. Then, by moving down the sample-holder to fully contact the cryogenic stage, the sample will be cooled down to a very low temperature, together with the stage. The sample is heated via a sample heater, while a nearby sample movement motor regulates the heating and cooling rates of the samples.

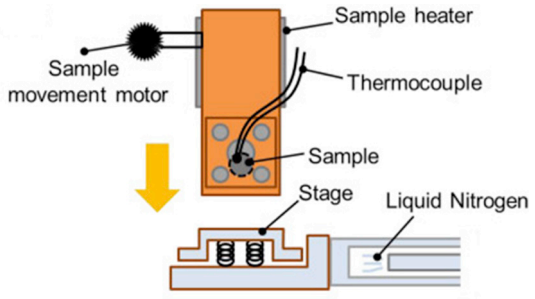

Fig. 6 Schematic of originally developed thermal treating instrument for deep cryogenic cycling [42]

2 Effects of deep cryogenic cycling parameters

As shown in Fig. 5, many parameters during deep cryogenic cycling affect the rejuvenation behavior, such as cycling number (N), the upper limit temperature (T_a), the lower limit temperature (T_b), the holding time in each temperature (t_a and t_b), and the cooling/heating rate.

2.1 Cycling number

GU et al [43] treated $Ti_{50}Zr_{20}Be_{20}Ni_{10}$ (at.%) via cryogenic thermal cycling in ambient atmosphere. The as-cast MGs were put in the boiling water (373 K) for 1 min and then put into liquid nitrogen (77 K) for 1 min, as shown in Fig. 7(a). The samples were treated for 15 and 30 cycles. They found that the structural relaxation enthalpy (ΔH) improved with a higher cycling number, as shown in Fig. 7(b). The value of ΔH increases from 4.45 J/g (as-cast sample) to 5.79 J/g (30 cycles), which also induced more free volume into the glassy matrix. However, for different alloy systems of metallic glasses, the change of ΔH after deep cryogenic cycle treatment is different.

GONG et al [44] investigated the rejuvenation of high-entropy bulk metallic glass (HE-BMGs) via cryogenic cycling treatment. $Ti_{20}Zr_{20}Hf_{20}Be_{20}Cu_{20}$ (at.%) MGs were put in liquid nitrogen for 10 min, and then heated to ambient temperature and held for 10 min. The samples were treated for 5, 10, 15, and 20 cycles. As shown in Fig. 8, the relaxation

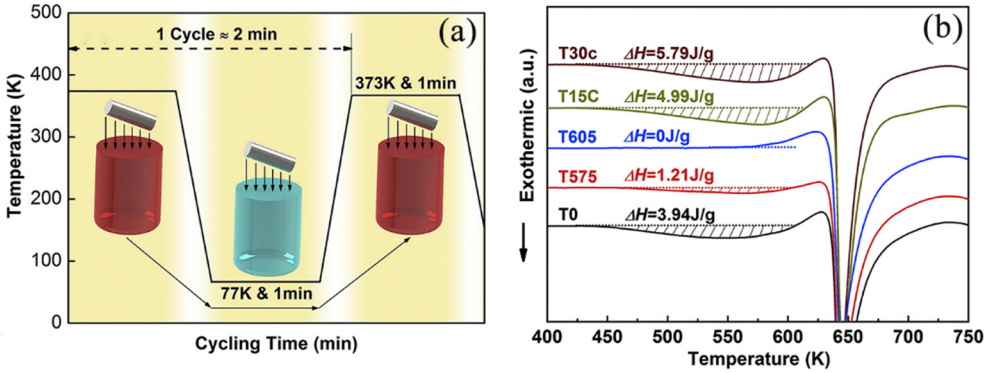

Fig. 7 Illustration of cryogenic thermal cycling process (a); DSC curves of $Ti_{50}Zr_{20}Be_{20}Ni_{10}$ MG in as-cast, annealed and cryogenic thermal cycling treated states (The structural relaxation enthalpy, ΔH, can be determined by integrating the area of exothermic peaks prior to glass transition event) (b) [43]

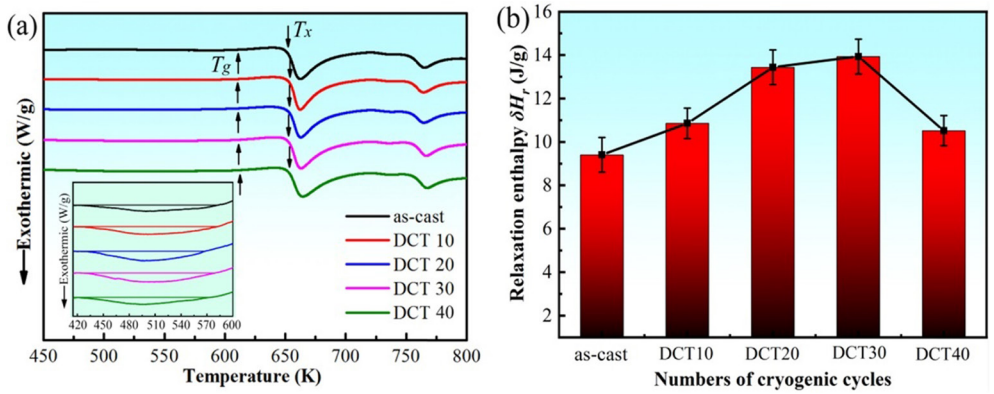

Fig. 8 DSC curves of as-cast and treated $Ti_{33}Zr_{30}Cu_9Ni_{5.5}Be_{22.5}$ MGs (The inset shows enlarged part in DSC curves) (a); Dependence of relaxation enthalpy on cycling numbers (b) [44]

enthalpy (ΔH) after deep cryogenic cycle treatment is higher than that of as-cast samples (4.376 J/g), which attributes to the induced free volume in the treated samples. However, ΔH reached the highest value at 10 cycles (5.964 J/g) and then decreased slightly when subjected to 20 cycles (5.279 J/g). LV et al [45] investigated the effects of deep cryogenic cycle treatment (DCT) on $Ti_{33}Zr_{30}Cu_9Ni_{5.5}Be_{22.5}$ bulk metallic glass. The specimens were treated for 10, 20, 30, and 40 cycles. The specimens were firstly dipped into liquid nitrogen for 10 min and then immersed in a 303 K constant-temperature water bath for 10 min. The specimen treated with 30 cycles exhibited a more prominent rejuvenation behavior manifested by a higher relaxation enthalpy (ΔH=13.93 J/g). When the cycling numbers were increased to 40, ΔH decreased to 10.42 J/g.

For the metallic glasses studied so far, the relaxation enthalpy after different cycling numbers is higher than that of the as-cast samples, which indicates that the samples rejuvenate during cryogenic cycling. However, the reason of the downtrend of some alloys treated with higher cycling numbers needs more in-depth studies.

2.2 Holding time

GUO et al [46] studied Zr−Cu−Al−Ni MGs by changing the holding time in the cryogenic temperature. The as-cast sample was held at 100 K for 7.5 h (the total time of 30 cycles), and then heated to room-temperature without cycling. The results clarified that no rejuvenation occurs without cyclic treatment because of the lack of internal stress. CHEN et al [47,48] investigated Cu−Zr−Ag−Al MGs with a relatively high glass forming ability. The as-cast samples were cooled to 80 K and kept at this temperature for different time (24, 96, 192, and 240 h). They found that the compressive fracture strength and the micro-hardness reach the highest value when the holding time was 192 h, and then it did not show significant change with cryogenic time. ZHANG et al [49] researched the rejuvenation behavior of heated samples subjected to cryogenic treatments (CTs) with different time intervals: 2 min, 12 h, 24 h, 48 h, and 96 h. The relaxation enthalpy (ΔH) of investigated samples is shown in Fig. 9. The liquid nitrogen quenching process can make the samples attain a less relaxed state with a higher ΔH. However, the subsequent CT has different effects on the relaxation enthalpy. The samples quenched from 333−353 K show a far lower relaxation enthalpy than the as-cast state, while they were rejuvenated with a longer cryogenic holding time. In contrast, the samples quenched from 373 or 393 K show the opposite trend. Interestingly, the samples quenched from various temperature reach the similar ΔH when the holding time is about 100 h.

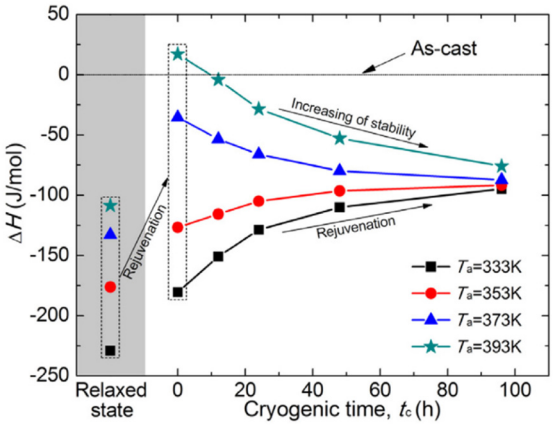

Fig. 9 Relative relaxation enthalpy of samples in relaxed and quenching + CT states obtained by subtracting enthalpy of as-cast sample [49]

The above study showed different trends of the samples with different cryogenic holding time, and these differences are also related to the composition and initial state of the samples. There are relatively few studies on the holding time at low temperature during cycling and it needs more research.

2.3 Cryogenic temperature range

GUO et al [46] studied Zr−Cu−Al−Ni MGs treated with 30 cycles at different cryogenic temperatures (220, 180, and 140 K). On the one hand, relaxation enthalpy (ΔH) of three samples, treated at 220, 180 and 140 K, were 13.4, 14.1, and 14.4 J/g, respectively. Apparently, with lower cryogenic temperature, the samples can be rejuvenated more. On the other hand, glass transition temperature (T_g) and onset crystallization temperature (T_x) are very similar for all samples, which indicates no great changes in the amorphous structure with various cryogenic temperatures. BIAN et al [50] investigated $Zr_{64.13}Cu_{15.75}Ni_{10.12}Al_{10}$ (at.%) MGs cooled to 77, 108, 123 and 153 K with a holding time of 1 h. The results of compressive tests demonstrated that the plasticity increased with

decreasing cryogenic temperature. When the cryogenic temperature decreased to 77 K, due to the gradual cooling contraction, the activation volume annihilates and some loosely packed regions are formed, which is in favor of the formation of flow units. Thus, more shear bands are activated at lower temperatures, which causes the insignificant serrated flow behavior with decreasing temperature.

The upper limit temperature was also studied. DI et al [51] treated $[(Fe_{0.5}Co_{0.5})_{0.75}B_{0.2}Si_{0.05}]_{96}Nb_4$ (at.%) MGs with cryogenic thermal cycling. The samples were treated for 15 cycles, in which the samples were firstly dipped into liquid nitrogen for 1 min, and then immersed in silicone oil at 433, 473, 513, 533, and 563 K (0.52−0.68 of T_g) for 1 min. As shown in Fig. 10, the improved ΔH suggests that rejuvenation occurs in all samples. The value of ΔH gradually increases with the temperature increasing from 433 to 533 K, and then decreases sharply when treated at 563 K. For the sample treated at 563 K, some larger nanocrystals extending to 2−3 nm were observed in the structure, so the evolution of $Fe_{23}B_6$ crystalline phase occurs after the deep cryogenic treatment, resulting in the different behaviors for other samples.

LIU et al [52] studied the rejuvenation behavior of La-based MGs via CTC (cryogenic treated cycling) treatment. $La_{60}Ni_{25}Al_{15}$ (at.%) MGs were dipped into liquid nitrogen for 1 min, and then immersed in ice water (273 K, $0.59T_g$) or boiling water (373 K, $0.81T_g$) for another 1 min. All samples were treated with 15 cycles. Figure 11(a) shows the results of DSC measurements. The sample obtained in the boiling water shows a lower ΔH_{rel} (131.7 J/mol) than the as-cast sample (174.0 J/mol), which means that the relaxation occurs. Meanwhile, the samples treated in ice water shows a higher ΔH_{rel} (207.8 J/mol) than the as-cast state, indicating the rejuvenation behavior. The shear transformation zone (STZ, Ω) is shown in Fig. 11(b). The same trend with ΔH_{rel} is seen, i.e., relaxed sample (Ω=3.85 nm^3) < as-cast sample (Ω=4.30 nm^3) < rejuvenated sample (Ω=4.86 nm^3). However, as shown in Fig. 11(c), E_β (activation energy of β relaxation) shows different trends, i.e., relaxed sample (E_β=96.61 kJ/mol) > as-cast sample (E_β=89.91 kJ/mol) > rejuvenated sample (E_β= 84.59 kJ/mol). Compared to the as-cast samples, the rejuvenated samples possess larger STZ volume and lower E_β, as well as a more heterogeneous microstructure. In such case, the deep cryogenic cycling treatment could also relax the samples, the internal stress generated during cycling would assist the atoms to hop from one sub-basin to another, and would also help some densely packed atoms hop into the gulf and thus transform to a more ordered structure.

The temperature range and the selection of two temperature endpoints during the deep cryogenic cycling treatment are critical. At different temperatures, the rejuvenated effects change. For the current study concerned, the rejuvenation effects are better for those samples treated at lower deep cryogenic temperatures. However, in some compositions, the upper limit temperature of room temperature does not cause a change in their structure and thermal properties, and thus the temperature range is extended. The results also showed that the wider temperature range could also degrade the rejuvenation behavior, which needs more in-depth study.

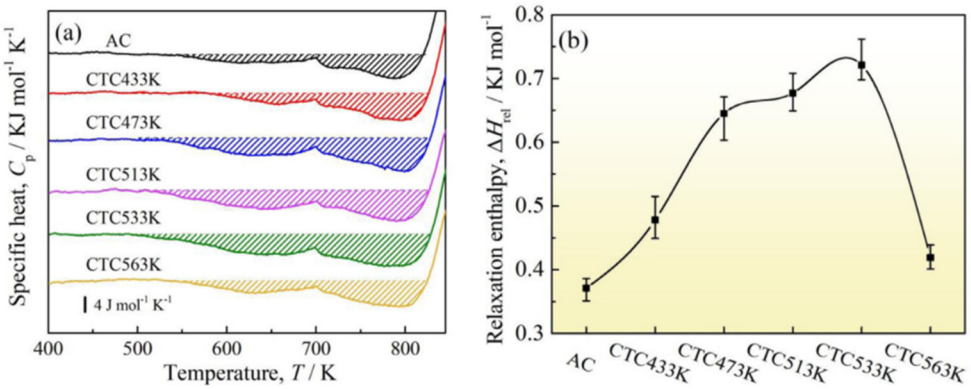

Fig. 10 Relaxation spectra (a) and variation of ΔH_{rel} (b) for AC (as-cast) and CTC (cryogenic treated cycles) treated $[(Fe_{0.5}Co_{0.5})_{0.75}B_{0.2}Si_{0.05}]_{96}Nb_4$ BMG samples [51]

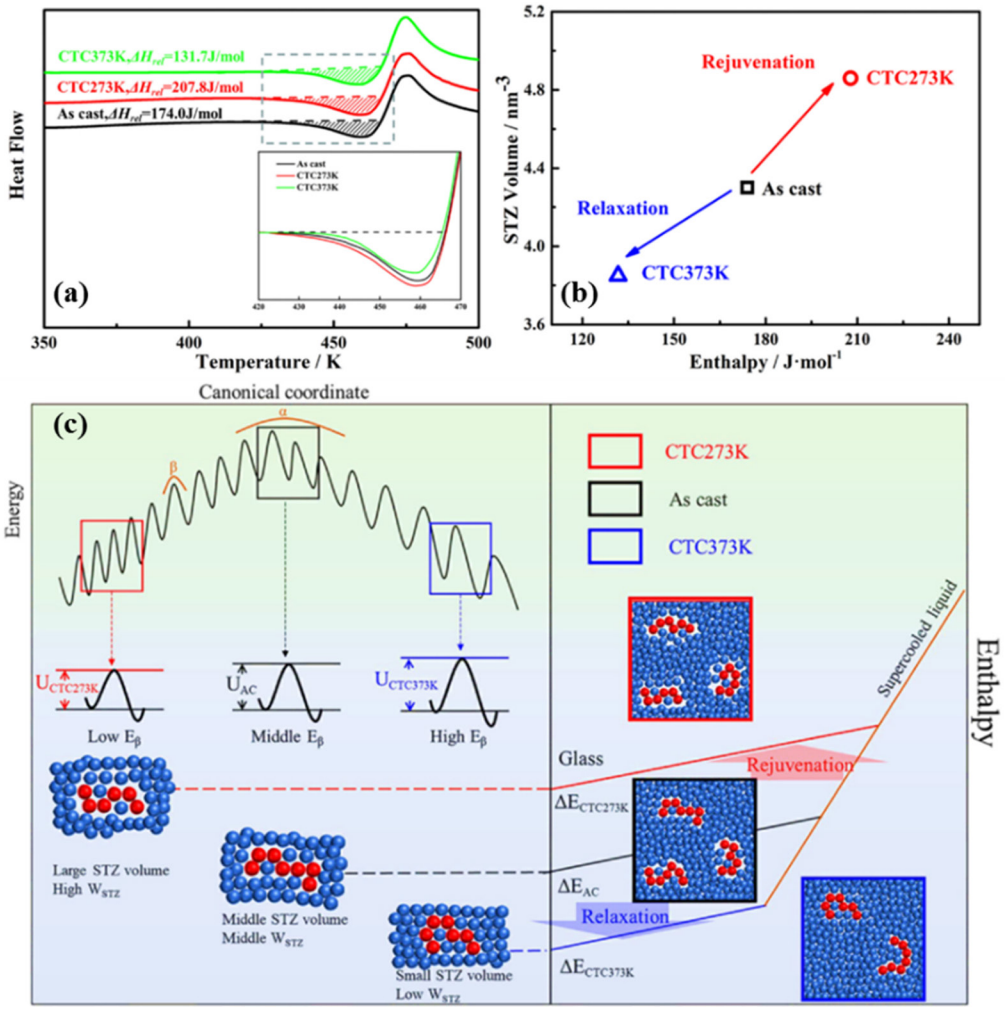

Fig. 11 DSC thermograms of as-cast and CTC treated specimens of LaNiAl MGs (a); STZ volume of as-cast and CTC treated specimens (b); Schematic illustration of relation between β relaxation and shear transformation zone (c) [52]

2.4 Heating/cooling rates

GUO et al [46] changed the cooling and heating rates during cycling. The heating and cooling rates were decreased to ~20 and 25 K/min. As shown in Fig. 12, the high-resolution TEM (HRTEM) images reveal that the treated sample shows a monolithic amorphous phase without nano-sized clusters or crystals. The value of ΔH has no obvious difference from that of the as-cast sample, which demonstrated that the heating/cooling rates would not play an important role in the rejuvenation.

SHANG et al [53] simulated the cryogenic cycling treatment on $Cu_{50}Zr_{50}$ (at.%) metallic glass. The initial samples were set with different quenching rates (10^9, 10^{10}, 10^{11}, 10^{12} or 10^{13} K/s), and the cooling and heating rates were varied from 5×10^{14} to 10^{13} K/s, respectively. As shown in Fig. 13, the results show that when the heating and cooling rates are much higher than those of the as-cast state, the sample rejuvenates. The initial potential energies are indicated by the arrows, the cryogenic holding time equal to 200 ps. When cooling rate during cycling (Q_b) to the initial cooling rate (Q_5) was 25, the samples after treatment were apparently relaxed; when $Q_b/Q_4>$ 250, the sample after treatment were rejuvenated. The greater the difference between the cooling rate during cycling and that of initial casting is, the higher the degree of rejuvenation is. However, as the cycling number increases, the potential energy of all samples finally tends to be the similar value.

To date, there have been relatively few experimental studies on the effects of heating and cooling rates during deep cryogenic cycling treatment. Even though it was found that a higher cooling rate would contribute to a higher degree of rejuvenation by simulation, the experimental investigation needs further study.

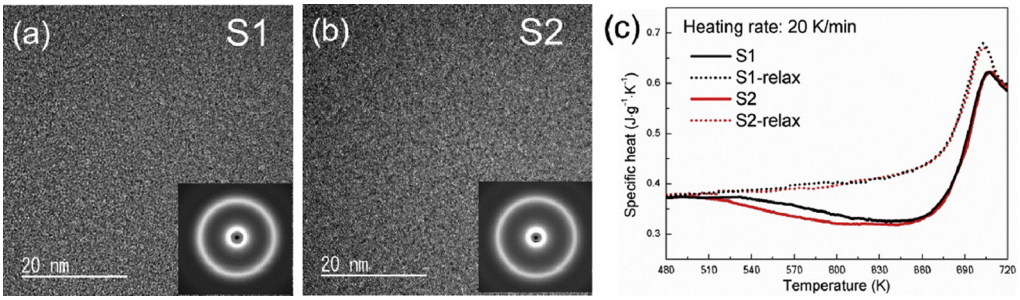

Fig. 12 High-resolution TEM images of S1 (lower heating rates) (a) and S2 (lower cooling rates) (b); Specific heat curves of S1 and S2, as well as their relaxed state (c) [46]

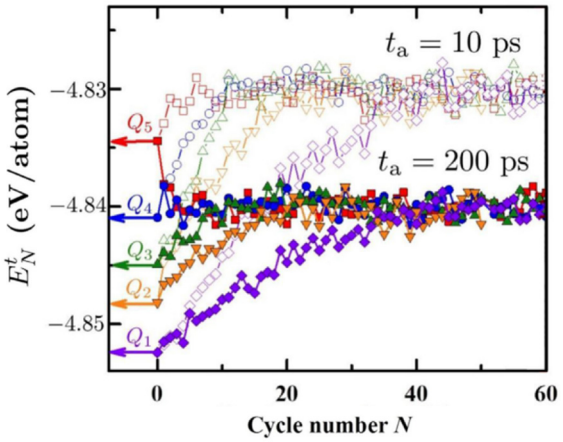

Fig. 13 Evolution of potential energy E_N^t, as function of cycle number N for samples with t_a=10 ps or 200 ps (The initial quenching rates are: Q_1=10^9 K/s, Q_2=10^{10} K/s, Q_3=10^{11} K/s, Q_4=10^{12} K/s, and Q_5=10^{13} K/s; T_a=400 K, t_b=100 ps, T_b=1 K, Q_a and Q_b=2.5×10^{14} K/s) [53]

3 Effects of initial state of treating samples

3.1 Composition of samples

GUO et al [54] reported that deep cryogenic cycling treatment did not affect the rejuvenation and plasticization of a Pd−Cu−Ni−P MG. They attributed such insensitivity upon cryogenic cycling to the more rigid cage structures and lower volume of free volume (lower heterogeneity) when compared to Zr-based MG. Such phenomenon may also be related with the fragility of the alloy system, i.e., Zr-based MGs are typically strong while Pd-based ones are typically fragile. Local atomic rearrangement can be interpreted by the cage theory, which suggests that some loosely-packed region is embedded in the densely packed matrix and the free volume in the cage is locked by the surrounding atoms, as shown in Fig. 14(b).

TANG et al [55] proposed a schematic picture to describe the evolution of atomic packing structure and mechanical behaviors of $Fe_{80}P_{20}$ MG during cryogenic-thermal cycling. As shown in Fig. 15, the microstructure of the as-cast MG possesses a larger scaled spatial heterogeneity, and the P-rich core regions coincide with open volume regions (OVRs). P atoms in the core regions are in a high energy state and the mobility of them is high. In contrast, Fe-rich shell regions might be in a low energy state, and the mobility is relatively low. During the cycling, the original loosely-packed cores of P atoms relax to a low-energy state. Meanwhile, the densely-packed shell of Fe atoms rejuvenates to a high-energy state. The distinctly large-sized OVRs in P-rich core regions shrink in size. Consequently, the relaxation in the sample could be predominant with cycling.

SOHRABI et al [56] used the raw La with different purity levels as starting materials to investigate the effects of deep cryogenic cycling treatment on the chemical heterogeneity. The $La_{60}Al_{25}Ni_{15}$ ingots prepared from high purity (La-HP) and low purity (La-LP) were dipped into liquid nitrogen (77 K) for 1 min and then quickly heated to 300 K and held for 1 min, and this cycle was repeated for intended numbers. As shown in Fig. 16, when the cycling number is up to 5, ΔH_{rel} of La-HP almost shows no change, while the increase of ΔH_{rel} of La-LP is larger than 80 J/mol. The results showed that the sample using low purity raw materials is more easily rejuvenated. The thermal stability against crystallization is degraded in La-LP. The control of chemical heterogeneity by adjusting the sample composition to regulate the rejuvenation behavior may be a feasible way to obtain the desired property of MGs.

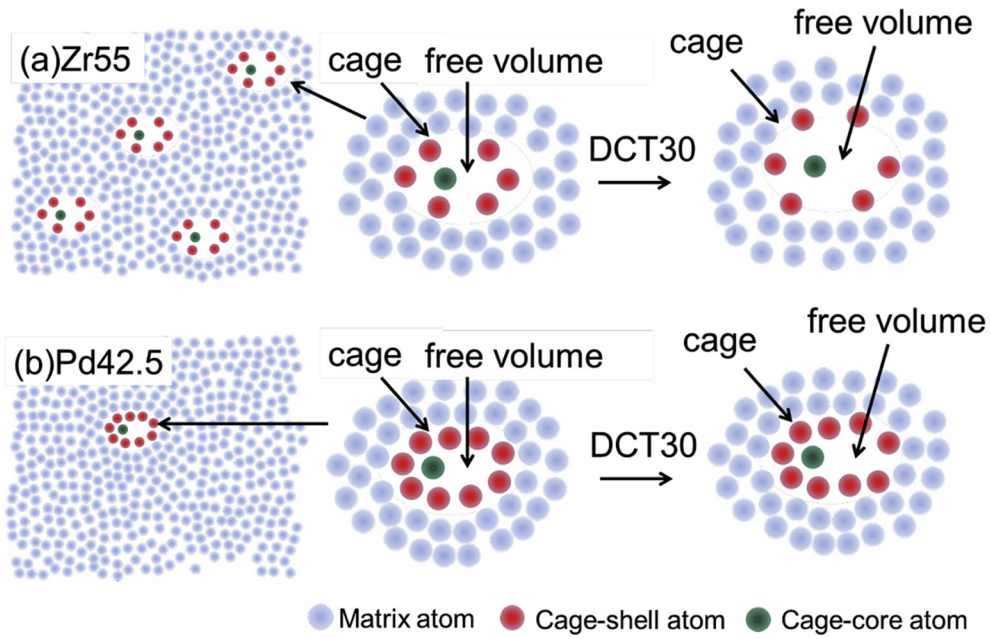

Fig. 14 Schematic illustration of different cage structures in Zr55 (a) and Pd42.5 (b) (For Zr55, more free volume is locked in cages and cage is not so rigid, and thus during cryogenic cycling, cage enlarges to induce free volume and rejuvenate sample; for Pd42.5, less and rigid cages make the structure difficult to change and no rejuvenation occurs) [54]

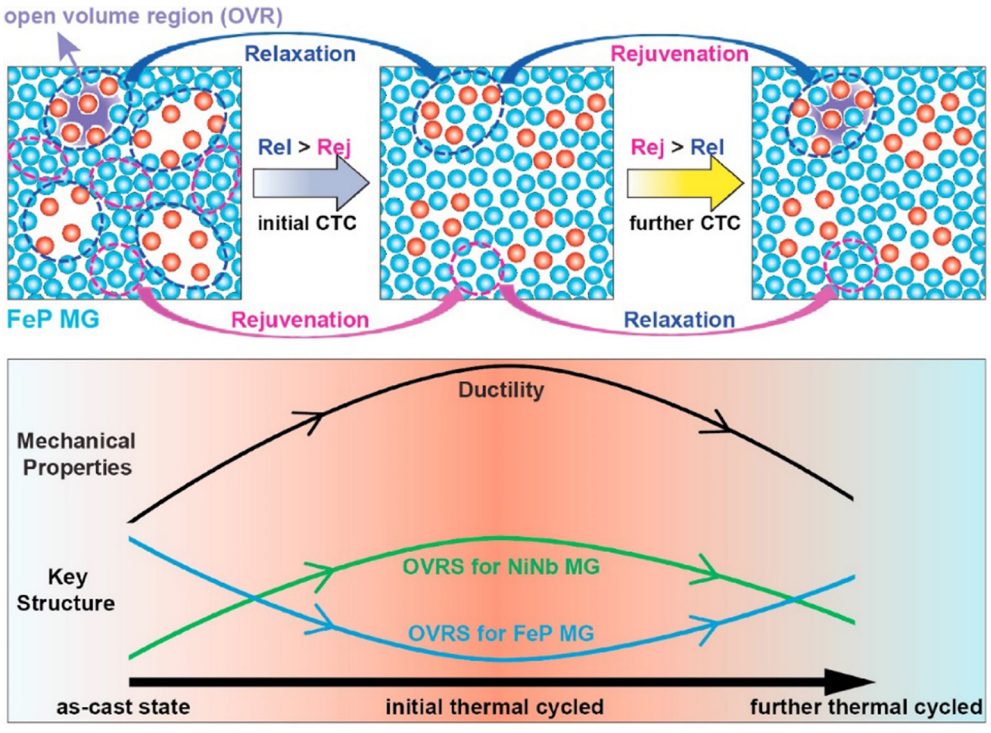

Fig. 15 Correlation map during thermal cycling and evolution of atomic packing structure and mechanical behaviors with thermal cycling established for $Fe_{80}P_{20}$ (P-rich core (red) and Fe-rich shell (blue) regions) [55]

3.2 Initial relaxation state

XIAO et al [41] studied the effects of pre-annealing before deep cryogenic cycling treatment on the structure and mechanical properties of $La_{62}Al_{14}Ag_{2.34}Ni1_{0.83}Co_{10.83}$ MGs. The as-cast sample was annealed at 400 K (~$0.9T_g$) for 3 days (fully relaxed sample). The as-cast sample and annealed sample were dipped into liquid nitrogen

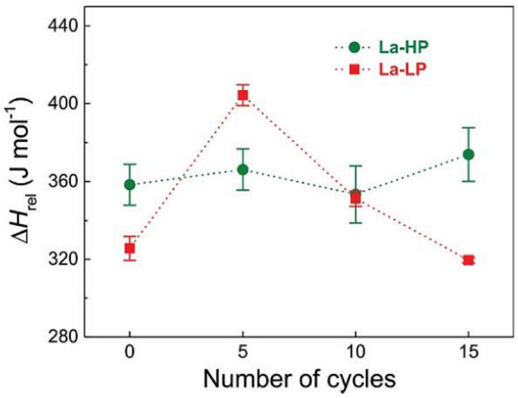

Fig. 16 Relaxation enthalpy as function of number of cycles for both La-HP and La-LP [56]

(77 K) for 2 min and then into alcohol (303 K) for 2 min, and such treatment was repeated for 120 cycles totally. As shown in Fig. 17(a), the value of ΔH_{rel} rapidly increased within 20 cycles and showed no obvious change after 20 cycles for the as-cast sample. In contrast, the annealed sample has no obvious changes and no rejuvenation behavior occurred. The results indicated that the long-time annealing not only annihilates the excess free volume, but also improves the local atomic ordering, thereby causing little changes in properties such as hardness, and Young's modulus, as shown in Figs. 17(b−f).

KANG et al [57] investigated the effects of different degrees of relaxation on the rejuvenation behavior during deep cryogenic cycling treatment. The as-cast $Zr_{46}Cu_{38}Al_8Ag_8$ (at.%) samples were pre-annealed at 639 K (~0.9T_g) for different durations (2−240 h) to produce the samples with various initial relaxation states. The deep cryogenic cycles were treated up to 20 cycles, in which one

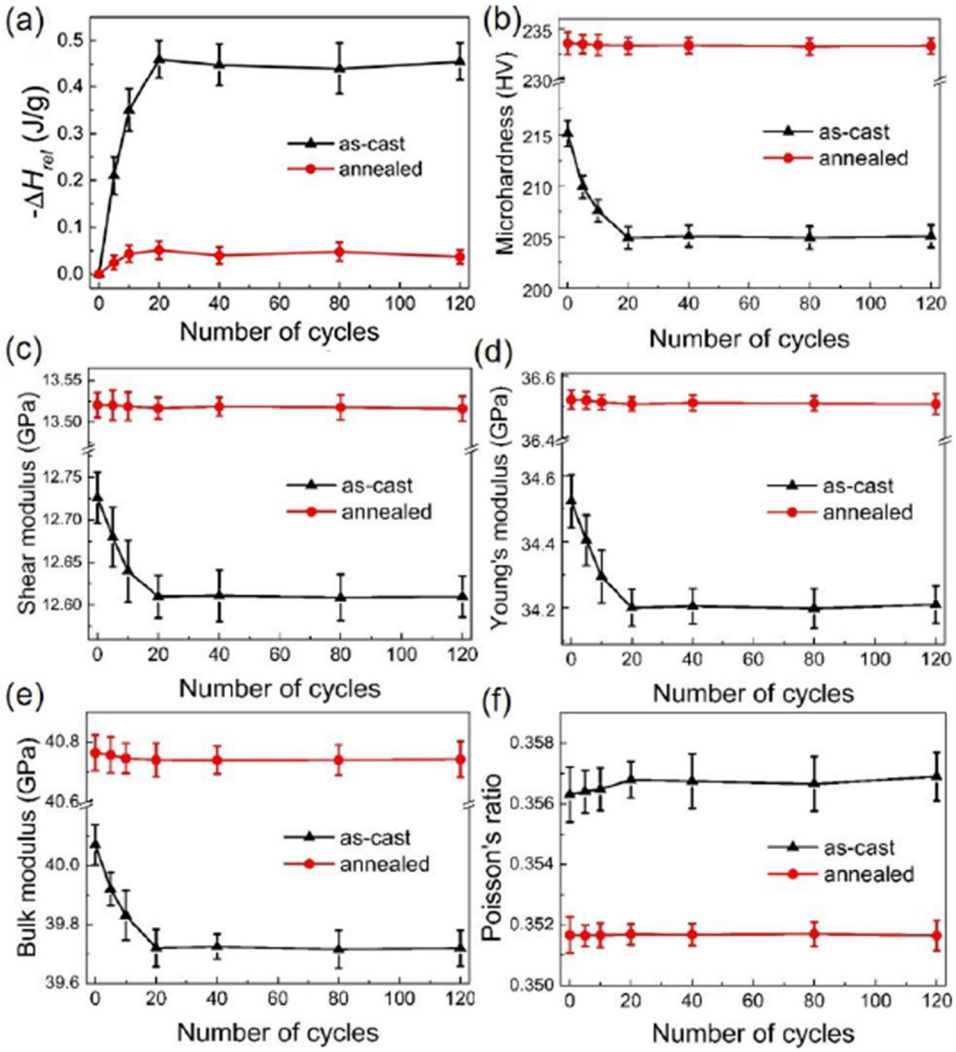

Fig. 17 Average values of relaxation enthalpy (a), microhardness (b), shear modulus (c), Young's modulus (d), bulk modulus (e) and Poisson's ratio (f) for as-cast and annealed MGs with different thermal cycles [41]

cycle was dipped into liquid-nitrogen (77 K) and then into boiling water (373 K). Figure 18(a) showed that the value of recovery enthalpy sharply increased when the pre-annealing time is below 20 h. After that, the growth rate is lower. The stress−strain curves during compression tests are shown in Fig. 18(b). The annealed samples exhibit no plasticity, while the cycling treated samples show limited plasticity. In addition, the samples with a longer annealing time or a higher degree of relaxation show lower plastic strain after cycling treatment. These results indicate that the pre-annealing treatment caused the annihilation of free volume, making structure more homogenous and thus more difficult to rejuvenate.

Above all, short-time annealed MG sample, which contains more free volume and possesses a higher structural heterogeneity, may be in favor of rejuvenating the samples. KETOV et al [13] found the same phenomenon in $Cu_{46}Zr_{46}Al_7Gd_1$ (at.%) MGs. The fully annealed (relaxed) sample (after DCT) is more brittle than the as-cast sample, while the partially annealed samples (after DCT) show a significant improvement in plasticity, even higher than the as-cast sample (after DCT). KETOV et al [13] also prepared rod-shaped samples of $Zr_{62}Cu_{24}Fe_5Al_9$ MGs with three diameters: 1.5, 2.0 and 2.5 mm. Certainly, a smaller sample means a higher cooling rate and a higher energy state. All samples were inserted into liquid nitrogen (77 K) for 1 min, and then into the ethanol (333−334 K) for 1 min, and this treatment was repeated for 60 cycles. The plastic strain of 1.5 mm in diameter samples is improved from 4.9% to 7.6% after cryogenic cycling treatment. Meanwhile, samples with larger size show limited improvements in plasticity. The differences in the degree of rejuvenation and improvement in mechanical property between samples with different sizes are related to the more relaxed state or more homogenous structure in the larger samples.

A summary of thermal properties of samples during deep cryogenic cycling treatment is given in Table 1.

4 Effects of deep cryogenic cycling treatment on properties

4.1 Mechanical properties

Deep cryogenic treatment often causes local atomic rearrangement in amorphous alloys, and the microstructure in different energy states is different, which results in various mechanical behaviors [60−63].

GUO et al [58] investigated the mechanical properties of $(Zr_{55}Cu_{30}Al_{10}Ni_5)_{100-x}Ta_x$ (at.%) (x=1, 3 and 5) (denoted as Ta1, Ta3 and Ta5), during cryogenic cycling treatment. The compressive stress−strain curves of the as-cast state and treated samples are shown in Fig. 19(a). All treated samples showed higher fracture strength and larger plastic strain compared with the as-cast samples. Figure 19(b) shows SEM image for the fracture surface of treated Ta5 samples, which exhibits well multiplied shear bands. The decrement in hardness (HD) in nano-indentation usually results from the more induced free volume. A quantitative calculation of the relationship between hardness and free volume is [64]

$$\mathrm{HD} = AT\sinh^{-1}\left[B\dot{\gamma}\exp\left(\frac{\Delta G}{k_\mathrm{B}}+\frac{\gamma v^*}{v_\mathrm{f}}\right)\right] \quad (1)$$

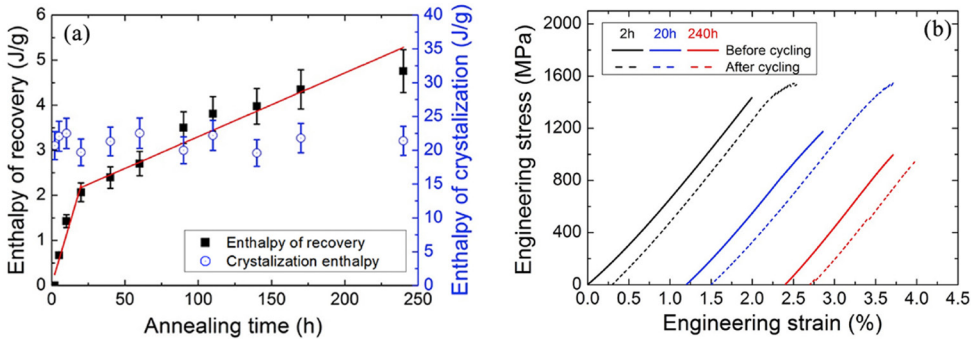

Fig. 18 Experimental data for cycling treated $Zr_{46}Cu_{38}Al_8Ag_8$ MGs with different pre-annealing durations: (a) Enthalpy of recovery and enthalpy of crystallization; (b) Representative stress−strain curves for samples with different pre-annealing time and cryogenic cycling treatment [57]

Table 1 Summary of thermal properties of samples during deep cryogenic cycling treatment

Composition/at.%	Sample morphology	Cycling number	Relaxation enthalpy	Ref.
$(Zr_{55}Cu_{30}Al_{10}Ni_5)_{99}Ta_1$	Rod	0	13.6 J/g	[58]
		30	15.7 J/g	
$(Zr_{55}Cu_{30}Al_{10}Ni_5)_{97}Ta_3$	Rod	0	9.2 J/g	[58]
		30	10.8 J/g	
$(Zr_{55}Cu_{30}Al_{10}Ni_5)_{95}Ta_5$	Rod	0	10.8 J/g	[58]
		30	12.8 J/g	
$Zr_{55}Cu_{30}Al_{10}Ni_5$	Rod	0	12.7 J/g	[42]
		30	14.6 J/g	
$Pd_{42.5}Cu_{30}Ni_{7.5}P_{20}$	Rod	0	9.468 J/g	[54]
		30	9.462 J/g	
$Ti_{50}Zr_{20}Hf_{20}Be_{20}Cu_{20}$	Rod	0	4.376 J/g	[44]
		5	5.802 J/g	
		10	5.964 J/g	
		15	5.237 J/g	
		20	5.279 J/g	
$Ti_{33}Zr_{30}Cu_9Ni_{5.5}Be_{22.5}$	Rod	0	9.41 J/g	[45]
		10	10.86 J/g	
		20	13.43 J/g	
		30	13.92 J/g	
$Ti_{41}Zr_{25}Be_{29}Al_5$	Rod	0	7.54 J/g	[59]
		80	7.19 J/g	
		200	6.23 J/g	
		400	6.18 J/g	
$La_{60}Ni_{25}Al_{15}$	Plate	0	17.4 J/g	[52]
		15	13.2 J/g	
$La_{60}Ni_{25}Al_{15}$ (High purity raw material 99.5%)	Rod	0	326 J/mol	[56]
		5	404 J/mol	
	Ribbon	0	839 J/mol	[56]
		5	846 J/mol	
$La_{60}Ni_{25}Al_{15}$ (Low purity raw material 98.9%)	Rod	0	358 J/mol	[56]
		5	366 J/mol	
	Ribbon	0	820 J/mol	[56]
		5	963 J/mol	

where A and B are constants; T is temperature; $\dot{\gamma}$ is the shear strain rate; ΔG is the activation barrier energy for defect migration; k_B is the Boltzmann constant; v_f is the average free volume per atom; γ is the correction term for the free volume overlap; v^* is the critical value of free volume for atomic diffusion.

The reduced free volume (x) [65,66] is calculated as [67]

$$x=v_f/\gamma v^*=2(\rho_c-\rho)/\rho \quad (2)$$

where ρ is the density of the sample, and ρ_c is the density of a sufficiently crystallized counterpart. It was also demonstrated that shear band [68] formation and free volume generation are correlated. Numerous shear bands nuclei are formed in the soft regions with more free volume. Above all, MGs possessing a more heterogeneous structure and more free volume show better mechanical properties after treatment. The detailed data of the mechanical properties are listed in Table 2. It can be seen that the mechanical properties of Zr-based

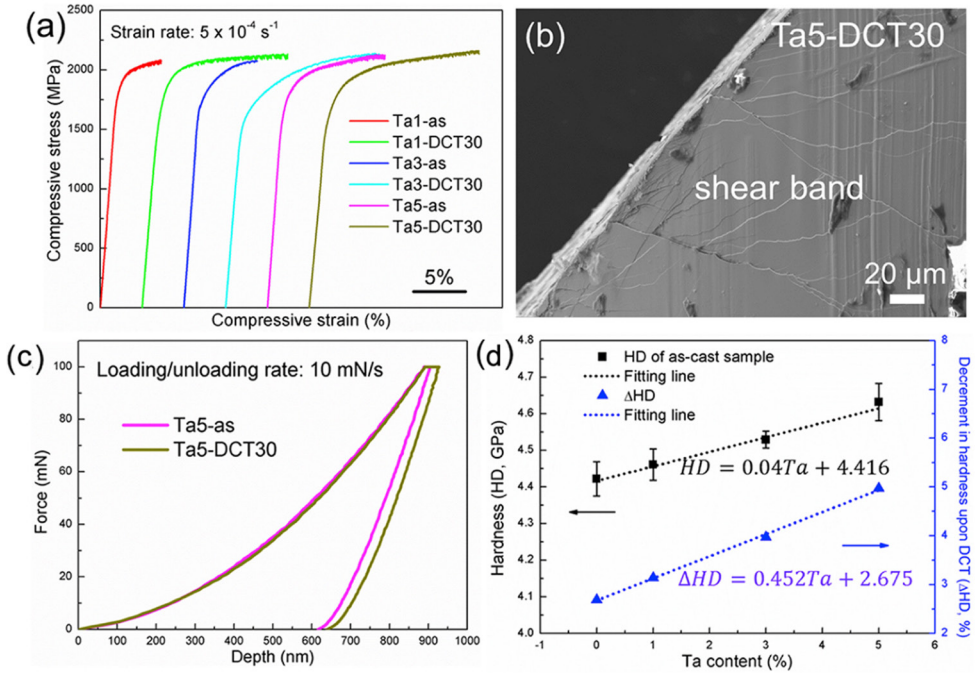

Fig. 19 Compressive stress−strain curves for Ta1/3/5-as and Ta1/3/5-DCT30 (a); SEM image of fracture surface for Ta5-DCT30 (b); Force−depth curves of Ta5-as and Ta5-DCT30 (c); Hardness (HD) and decrement in HD (ΔHD) upon DCT, as function of Ta content (d) [58]

Table 2 Summary of mechanical data during cryogenic cycling treatment

Composition/at.%	Cycling number	Nano-indentation		Compression testing				
		h_{max}/nm	H/GPa	E/GPa	σ_f/MPa	σ_y/MPa	ε_f/%	ε_p/%
$(Zr_{55}Cu_{30}Al_{10}Ni_5)_{99}Ta_1$	0	921	4.461	116	2080	1660	5.8	4.4
	30	936	4.321	106	2132	1440	13.9	12.5
$(Zr_{55}Cu_{30}Al_{10}Ni_5)_{97}Ta_3$	0	914	4.529	117	2072	1638	7	5.6
	30	938	4.349	106	2133	1520	14.7	13.1
$(Zr_{55}Cu_{30}Al_{10}Ni_5)_{95}Ta_5$	0	904	4.632	119	2122	1620	10.5	9
	30	927	4.402	108	2161	1568	16.2	14.4
$Zr_{55}Cu_{30}Al_{10}Ni_5$	0	925	4.422	115	2070	1876	6.6	4
	30	937	4.303	106	2165	1706	12.7	11
$Pd_{42.5}Cu_{30}Ni_{7.5}P_{20}$	0	940	4.281	100	1842	1262	4.6	3.3
	30	944	4.427	105	1844	1281	4.1	2.6
$Ti_{20}Zr_{20}Hf_{20}Be_{20}Cu_{20}$	0	190.2	7.99	123	1990	2027	–	0.62
	5	192.1	7.85	121	1818	2007	–	2.1
	10	193.2	7.75	128	1807	2076	–	3.11
	15	196.9	7.66	128	1820	2081	–	3.64
	20	200.7	7.38	125	1831	2114	–	5.38
$Ti_{33}Zr_{30}Cu_9Ni_{5.5}Be_{22.5}$	0	–	7.56	112.2	2018	1870	–	1.4
	10	–	7.46	110.5	–	–	–	–
	20	–	7.38	109.7	–	–	–	–
	30	–	7.3	109.5	2042	1819	–	7.8
	40	–	7.54	110.9	–	–	–	–

h_{max}: Maximum depth; H: Hardness; E: Elastic modulus; σ_f: Fracture stress; σ_y: Yielding stress; ε_f: Fracture strain; ε_p: Plastic strain

MGs [23,69,70] and La-based MGs [56] are widely studied, including the composition, cycling number and temperature range. The improvement of mechanical properties of Ti-based MGs [71] is widely studied in terms of cycle number. Due to the "denser" structure of Pd-based MGs, the mechanical properties show insignificant change. DING et al [72] investigated the stress boundary mechanism between structural rejuvenation and ageing via a theoretical constitutive model systematically, based on a framework of shear transformation and free volume. Beyond the stress threshold, the generation of free volume induced by explosive shear transformations overwhelms its annihilation, leading to the structural rejuvenation.

4.2 Magnetic properties

RI et al [73] investigated the changes on soft magnetic properties of Fe-based MGs after the cryogenic cycling treatment. $Fe_{78}Si_9B_{13}$ (at.%) ribbons were pre-annealed at 390 °C for 2 h under Ar atmosphere, then cycled from 300 to 77 K and the holding time of cycling is 1 min. Figure 20 shows the changes of magnetic induction B_m and coercivity H_c during cryogenic cycling. B_m and H_c showed complicated behavior with more cycling numbers. The magnetic anisotropy fluctuated as a consequence of the local structural changes, including the change in topological short-range order or the number of nearest neighbors.

RI et al [74] also investigated the changes of soft magnetic properties of Fe-based MGs by acyclic liquid nitrogen (LN) treatment. They used the same composition ribbons that were pre-annealed below the Curie temperature (663 K) for 1 h, and then treated at a cryogenic temperature for 60 d. As shown in Figs. 21(a, b), with a longer treating time, the Curie temperature (T_c) firstly moved to a lower value, subsequently rose to a higher value, and the values had no obvious change after 30 d. Meanwhile, the value of B_m and H_c showed an overall increasing and decreasing trend, respectively. The acyclic liquid nitrogen (LN) treatment induced structural changes and improved magnetic permeability in the rejuvenated samples. Above all, the cycling numbers and the holding time in liquid nitrogen affect the magnetic properties of the rejuvenated Fe-based amorphous alloy.

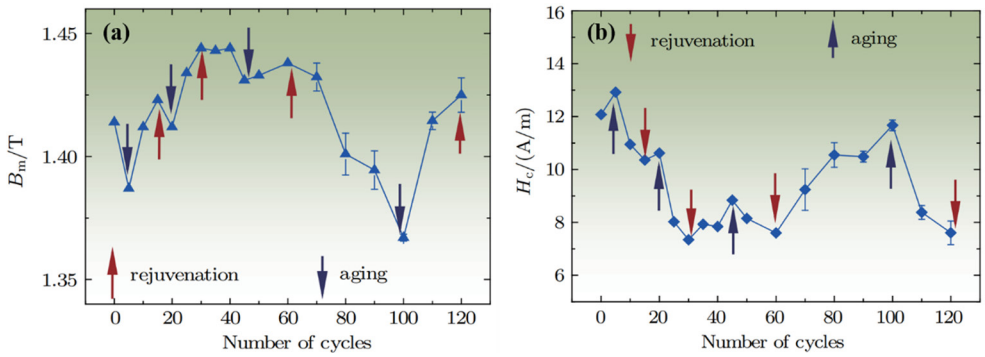

Fig. 20 Magnetic inductions (a) and magnetic coercivities (b) changing with cycling number during cryogenic cycling treatment [73]

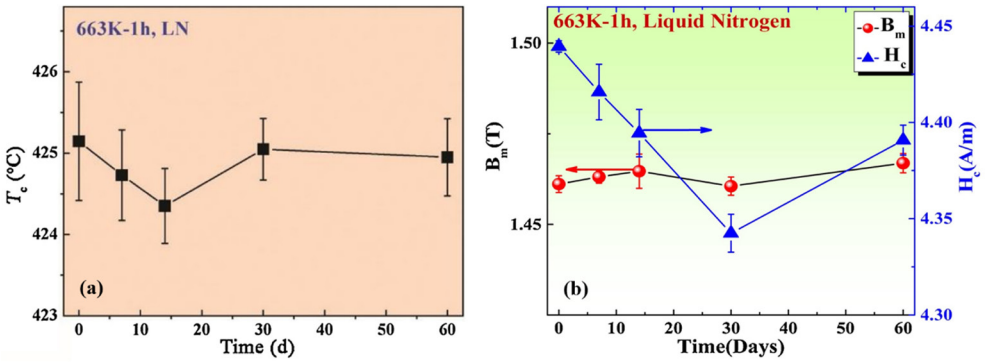

Fig. 21 Relations between treatment time and Curie temperature in $Fe_{78}Si_9B_{13}$ amorphous ribbons (a); Relations between magnetic induction and coercivity in $Fe_{78}Si_9B_{13}$ amorphous ribbons with treating time (b) [74]

4.3 Corrosion resistance

GU et al [43] investigated the electrochemical behavior of $Ti_{50}Zr_{20}Be_{20}Ni_{10}$ metallic glasses. The samples were cycled by inserting into water (373 K) for 1 min, and then inserting into liquid nitrogen for 1 min with 15 or 30 cycles. The structural relaxation enthalpy of the as-cast, annealed, and rejuvenated samples (15 and 30 cycles) were 4.45, 0.87, 4.99 and 5.79 J/g, respectively. Corrosion behavior of the samples were evaluated in 3.5 wt.% NaCl solution, and the rejuvenated samples performed contrary effects on corrosion resistance as compared with annealed samples. The cryogenic thermal cycling treatment helped to introduce more free volume into the as-cast sample, and the change of free volume deteriorated the stability of surface passive film.

5 Conclusions and remarks

The deep cryogenic cycling treatment could tailor Ti-based, Zr-based and La-based metallic glasses to a relatively higher energy state to modulate their internal structure and properties, especially the higher plastic deformability without changing the morphology of the samples. For metallic glasses with relatively high glass-forming ability, simple deep cryogenic cycling treatments can improve the structural inhomogeneity and thus achieve rejuvenation. At present, the related research is mainly focused on the process of how to obtain rejuvenated samples, while the influences of the initial intrinsic structural characteristics, as well as the interconnection of the property−rejuvenation−structure, have not been studied intensively and systematically.

From the view of properties, for metallic glasses, the low-temperature physical properties, such as the low-temperature specific heat, have received extensive attentions. Specific heat is one important macroscopic physical property and can contribute to the understanding of phase transitions. Meanwhile, the low-temperature bosonic peak and β-relaxation behavior are two important intrinsic kinetic behaviors in metallic glasses. Deep cryogenic cycling can change the content of free volume, which plays an important role in mechanical properties and atomic dynamics. Thus, it is important to clarify the effects of more induced free volume via thermal cycling on controlling the behavior of boson peaks and β-relaxation, as well as that on the atomic dynamics and structure.

From the view of structure, deep cryogenic cycling treatment causes the elevation of energy state, and the different energy states should exhibit different short-range ordered structures. However, there are few studies on the structural characterization.

Acknowledgments

This work was supported by the National Natural Science Foundation of China (No. 52101138), the Natural Science Foundation of Hubei Province, China (No. 2020CFB259), State Key Lab of Advanced Metals and Materials, China (No. 2020-Z01), State Key Laboratory for Mechanical Behavior of Materials, China (No. 20202205), State Key Laboratory of Advanced Design and Manufacturing for Vehicle Body, China (No. 32015001), and Guangdong Basic and Applied Basic Research Foundation, China (No. 2020A1515110531).

References

[1] GREER A L. Metallic glasses [J]. Current Opinion in Solid State and Materials Science, 1997, 2: 412−416.

[2] CHOI-YIM H, JOHNSON W L. Bulk metallic glass matrix composites [J]. Applied Physics Letters, 1997, 71: 3808−3810.

[3] WANG Wei-hua, DONG Chuang, SHEK C H. Bulk metallic glasses [J]. Materials Science and Engineering: R: Reports, 2004, 44: 45−89.

[4] CHENG Yong-qiang, MA E. Atomic-level structure and structure–property relationship in metallic glasses [J]. Progress in Materials Science, 2011, 56: 379−473.

[5] TREXLER M M, THADHANI N N. Mechanical properties of bulk metallic glasses [J]. Progress in Materials Science, 2010, 55: 759−839.

[6] WANG Wei-hua. The elastic properties, elastic models and elastic perspectives of metallic glasses [J]. Progress in Materials Science, 2012, 57: 487−656.

[7] SCULLY J R, GEBERT A, PAYER J H. Corrosion and related mechanical properties of bulk metallic glasses [J]. Journal of Materials Research, 2007, 22: 302−313.

[8] ZHOU Zhen-ya, PENG Hai-long, YU Hai-bin. Structural origin for vibration-induced accelerated aging and rejuvenation in metallic glasses [J]. Journal of Chemical Physics, 2019, 150: 204507.

[9] WANG Peng, YANG Xin-hua. Atomistic investigation of aging and rejuvenation in CuZr metallic glass under cyclic loading [J]. Computational Materials Science, 2020, 185: 109965.

[10] BRUNS M, HASSANI M, VARNIK F, HASSANPOUR A,

DIVINSKI S, WILDE G. Decelerated aging in metallic glasses by low temperature thermal cycling [J]. Physical Review Research, 2021, 3: 013234.

[11] ZHANG Lian-shun, WANG Tuo, HOU Qi-qi, HAO Qi, QIAO Ji-chao. Deformation-induced microstructural heterogeneity and rejuvenation in a Zr-based bulk metallic glass [J]. Journal of Non-Crystalline Solids, 2021, 574: 121148.

[12] KETOV S V, SUN Y H, NACHUM S, LU Zhen, CHECCHI A, BERALDIN A R, BAI Hai-yang, WANG Wei-hua, LOUZGUINE-LUZGIN D V, CARPENTER M A, GREER A L. Rejuvenation of metallic glasses by non-affine thermal strain [J]. Nature, 2015, 524: 200−203.

[13] WAKEDA M, SAIDA Jun-ji, LI Ju, OGATA S. Controlled rejuvenation of amorphous metals with thermal processing [J]. Scientific Reports, 2015, 5: 10545.

[14] MIYAZAKI N, WAKEDA M, WANG Yun-jiang, OGATA S. Prediction of pressure-promoted thermal rejuvenation in metallic glasses [J]. Npj Computational Materials, 2016, 2: 16013.

[15] QIAO Ji-chao, WANG Qing, PELLETIER J M, KATO H, CASALINI R, CRESPO D, PINEDA E, YAO Yao, YANG Yong. Structural heterogeneities and mechanical behavior of amorphous alloys [J]. Progress in Materials Science, 2019, 104: 250−329.

[16] TAO Kai, QIAO Ji-chao, HE Quan-feng, SONG Kai-kai, YANG Yong. Revealing the structural heterogeneity of metallic glass: Mechanical spectroscopy and nanoindentation experiments [J]. International Journal of Mechanical Sciences, 2021, 201: 106469.

[17] SONG Wen-li, MENG Xiao-he, WU Yuan, CAO Di, WANG Hui, LIU Xiong-jun, WANG Xian-zhen, LV Zhao-ping. Improving plasticity of the $Zr_{46}Cu_{46}Al_8$ bulk metallic glass via thermal rejuvenation [J]. Science Bulletin, 2018, 63: 840−844.

[18] JIANG Min-qiang, GAO Yang. Structural rejuvenation of metallic glasses and its effect on mechanical behaviors [J]. Acta Metallurgica Sinica, 2021, 57: 425−438. (in Chinese)

[19] DING Gan, JIANG Feng, DAI Lan-hong, JIANG Min-qiang. Effective energy density of glass rejuvenation [J]. Acta Mechanica Solida Sinica, 2022, 35: 746−754.

[20] SHAYAKHMETOV Y, VOROBEVA A, BURLANKOV S, BOGONOSOV K, FOMIN A, GONCHAROV A, KRASNIKOV S, NIKOLAEVA S, OVSYANNIKOVA A, ZEKIY A O, PANDEY M. Effect of surface mechanical attrition treatment on micro-mechanical properties of ZrCuAlNi bulk metallic glass [J]. Materials Research, 2021, 24: e20210105.

[21] WANG Ming-zi, LIU Hai-shun, Mo Jin-yong, ZHANG Yue, CHEN Zhe, YIN Chun-hao, YANG Wei-ming. Thermal-pressure effects on energy state of metallic glass $Cu_{50}Zr_{50}$ [J]. Computational Materials Science, 2018, 155: 493−498.

[22] WANG Ming-zi, LIU Hai-shun, Li Jing-yan, JIANG Qi, YANG Wei-ming, TANG Chun-guang. Thermal-pressure treatment for tuning the atomic structure of metallic glass Cu−Zr [J]. Journal of Non-Crystalline Solids, 2020, 535: 119963.

[23] TJAHJONO T, ELVENY M, IBRAHIM O A, SUHARNO, CHUPRADIT S, BOKOV D, HOI H T, PANDEY M. Role of cryogenic cycling rejuvenation on flow behavior of ZrCuAlNiAg metallic glass at relaxation temperature [J]. Transactions of the Indian Institute of Metals, 2021, 74: 3241−3247.

[24] SUN Qi-jing, MISKOVIC D M, KONG Hui, FERRY M. Transition from relaxation to rejuvenation in ultrastable metallic glass driven by annealing [J]. Applied Surface Science, 2021, 546: 149048.

[25] EBNER C, PAULY S, ECKERT J, RENTENBERGER C. Effect of mechanically induced structural rejuvenation on the deformation behaviour of CuZr based bulk metallic glass [J]. Materials Science and Engineering A, 2020, 773: 138848.

[26] ZHANG Meng, WANG Yi-mei, LI Fu-xiang, JIANG Shao-qin, Li Mao-zhi, LIU Lin. Mechanical relaxation-to-rejuvenation transition in a Zr-based bulk metallic glass [J]. Scientific Reports, 2017, 7: 625.

[27] YUAN Xu-dong, ŞOPU D, SONG Kai-kai, ECKERT J. Relaxation and strain-hardening relationships in highly rejuvenated metallic glasses [J]. Materials, 2022, 15: 1702.

[28] ZHANG Sai-long, SHI Bo, WANG Jin-hui, XU Yuan-li, JIN Pei-peng. Rejuvenation of a naturally aged bulk metallic glass by elastostatic loading [J]. Materials Science and Engineering A, 2021, 806: 140843.

[29] LOUZGUINE-LUZGIN D V, ZADOROZHNYY V Y, KETOV S V, WANG Zhi, TSARKOV A A, GREER A L. On room-temperature quasi-elastic mechanical behaviour of bulk metallic glasses [J]. Acta Materialia, 2017, 129: 343−351.

[30] DING Gan, LI Cheng, ZACCONE A, WANG Wei-hua, LEI He-chang, JIANG Feng, LING Zhong, JIANG Min-qiang. Ultrafast extreme rejuvenation of metallic glasses by shock compression [J]. Science Advances, 2019, 5: eaaw6249.

[31] LEE M H, LEE K S, DAS J, THOMAS J, KÜHN U, ECKERT J. Improved plasticity of bulk metallic glasses upon cold rolling [J]. Scripta Materialia, 2010, 62: 678−681.

[32] CONCUSTELL A, MÉAR F O, SURIÑACH S, BARÓ M D, GREER A L. Structural relaxation and rejuvenation in a metallic glass induced by shot-peening [J]. Philosophical Magazine Letters, 2009, 89: 831−840.

[33] MAHMOUD Z H, BARAZANDEH H, MOSTAFAVI S M, ERSHOV K, GONCHAROV A, KUZNETSOV A S, KRAVCHENKO O D, ZHU Yu. Identification of rejuvenation and relaxation regions in a Zr-based metallic glass induced by laser shock peening [J]. Journal of Materials Research and Technology, 2021, 11: 2015−2020.

[34] GUNDEROV D, ASTANIN V. Influence of HPT deformation on the structure and properties of amorphous alloys [J]. Metals, 2020, 10: 415.

[35] GUNDEROV D, BOLTYNJUK E, UBYIVOVK E, CHURAKOVA A, KILMAMETOV A, VALIEV R. Consolidation of the amorphous $Zr_{50}Cu_{50}$ ribbons by high-pressure torsion [J]. Advanced Engineering Materials, 2020, 22: 1900694.

[36] GUNDEROV D V, CHURAKOVA A A, ASTANIN V V, ASFANDIYAROV R N, HAHN H, VALIEV R Z. Accumulative HPT of Zr-based bulk metallic glasses [J]. Materials Letters, 2020, 261: 127000.

[37] MENG Fan-qiang, TSUCHIYA K, SEIICHIRO I I, YOKOYAMA Y. Reversible transition of deformation mode

by structural rejuvenation and relaxation in bulk metallic glass [J]. Applied Physics Letters, 2012, 101: 121914.

[38] LI Shuo, HUANG Ping, WANG Fei. Rejuvenation saturation upon cyclic elastic loading in metallic glass [J]. Computational Materials Science, 2019,166: 318−325.

[39] SAIDA Jun-ji, YAMADA R, WAKEDA M, OGATA S. Thermal rejuvenation in metallic glasses [J]. Science and Technology of Advanced Materials, 2017,18: 152−162.

[40] SAIDA Jun-ji, YAMADA R, WAKEDA M. Recovery of less relaxed state in Zr−Al−Ni−Cu bulk metallic glass annealed above glass transition temperature [J]. Applied Physics Letters, 2013,103: 221910.

[41] XIAO Hai-bin, WANG Xiao-dong, ZHANG Peng, CAO Xiao-zhong, CHEN Yu, LE Tian, CAO Qing-ping, ZHANG Dong-xian, JIANG Jian-zhong. Contribution of cryogenic thermal cycling to the atomic dynamics in a La-based bulk metallic glass with different initial states [J]. Journal of Applied Physics, 2020, 127: 205104.

[42] GUO Wei, YAMADA R, SAIDA Jun-ji. Rejuvenation and plasticization of metallic glass by deep cryogenic cycling treatment [J]. Intermetallics, 2018, 93: 141−147.

[43] GU Jia-lun, SHAO Yang, SHI Ling-xiang, SI Jia-jia, YAO Ke-fu. Novel corrosion behaviours of the annealing and cryogenic thermal cycling treated Ti-based metallic glasses [J]. Intermetallics, 2019, 110: 106467.

[44] GONG Pan, YIN Geng, JAMILI-SHIRVAN Z, DING Hong-yu, WANG Xin-yun, JIN Jun-song. Influence of deep cryogenic cycling on the rejuvenation and plasticization of TiZrHfBeCu high-entropy bulk metallic glass [J]. Materials Science and Engineering A, 2020, 797:140078.

[45] LV Jing-wang, WANG Fei-long, YIN Da-wei, ZHANG Shan, CAI Zheng-qing, SHI Zhi-lin, MA Ming-zhen, ZHANG Xin-yu. Effect of deep cryogenic cycling treatment on the microstructure and mechanical properties of Ti-based bulk metallic glass [J]. Journal of Alloys and Compounds, 2021, 887: 161386.

[46] GUO Wei, SHAO Yu-man, ZHAO Mi, LV Shu-lin, WU Shu-sen. Varying the treating conditions to rejuvenate metallic glass by deep cryogenic cycling treatment [J]. Journal of Alloys and Compounds, 2020, 819: 152997.

[47] CHEN Zhen-hua, ZHANG Li-ke, LIU Ji-zi, CHEN Ding. Cryogenic treatment induced hardening for Cu−Zr−Ag−Al bulk metallic glasses [J]. Science China Technological Sciences, 2013, 56: 637−641.

[48] ZHANG Li-ke, CHEN Zhen-hua, CHEN Ding, ZHENG Qun. Cryogenic treatment induced hardening of $Cu_{45}Zr_{45}Ag_7Al_3$ bulk metallic glass [J]. Physica B: Condensed Matter, 2014, 433: 84−88.

[49] ZHANG Wei, LI Ke-long, XIANG Qing-chun, REN Ying-lei, LI Qing-feng, QIU Ke-qiang. The rejuvenation and relaxation around the glass transition of a Ce-based metallic glass controlled by annealing, quenching and cryogenic treatments [J]. Journal of Non-Crystalline Solids, 2020, 548: 120334.

[50] BIAN Xi-lei, WANG Gang, WANG Qing, SUN Bao-an, HUSSAIN I, ZHAI Qi-jie, MATTERN N, BEDNARČIK J, ECKERT J. Cryogenic-temperature-induced structural transformation of a metallic glass [J]. Materials Research Letters, 2017, 5: 284−291.

[51] DI Si-yi, WANG Qian-qian, ZHOU Jing, SHEN Yi-yang, LI Jia-qi, ZHU Ming-yun, YIN Kui-bo, ZENG Qiao-shi, SUN Li-tao, SHEN Bao-long. Enhancement of plasticity for FeCoBSiNb bulk metallic glass with superhigh strength through cryogenic thermal cycling [J]. Scripta Materialia, 2020, 187: 13−18.

[52] LIU Zhen, HUANG Ping, WANG Fei. The correlation between β relaxation and shear transformation zone in LaNiAl bulk metallic glasses: The effect of cryogenic thermal cycling treatment [J]. Journal of Alloys and Compounds, 2021, 865: 158993.

[53] SHANG Bao-shuang, WANG Wei-hua, GREER A L, GUAN Peng-fei. Atomistic modelling of thermal-cycling rejuvenation in metallic glasses [J]. Acta Materialia, 2021, 213: 116952.

[54] GUO Wei, SAIDA Jun-ji, ZHAO Mi, LÜ Shu-lin, WU Shu-sen. Unconspicuous rejuvenation of a Pd-based metallic glass upon deep cryogenic cycling treatment [J]. Materials Science and Engineering A, 2019, 759: 59−64.

[55] TANG Yao, ZHOU Hao-fei, WANG Xiao-dong, CAO Qing-ping, ZANG Dong-xian, JIANG Jian-zhong. Origin of different thermal cycling effects in $Fe_{80}P_{20}$ and $Ni_{60}Nb_{40}$ metallic glasses [J]. Materials Today Physics, 2021, 17: 100349.

[56] SOHRABI S, RI M C, JIANG Hong-yu, GU Lin, WEN Ping, SUN Yong-hao, WANG Wei-hua. Prominent role of chemical heterogeneity on cryogenic rejuvenation and thermomechanical properties of La−Al−Ni metallic glass [J]. Intermetallics, 2019, 111: 106497.

[57] KANG Sang-jun, CAO Qing-ping, LIU Jian, TANG Yao, WANG Xiao-dong, ZHANG Dong-xian, AHN I S, CARON A, JIANG Jian-zhong. Intermediate structural state for maximizing the rejuvenation effect in metallic glass via thermo-cycling treatment [J]. Journal of Alloys and Compounds, 2019, 795: 493−500.

[58] GUO Wei, SHAO Yu-man, SAIDA J J, ZHAO Mi, LÜ Shu-lin, WU Shu-sen. Rejuvenation and plasticization of Zr-based bulk metallic glass with various Ta content upon deep cryogenic cycling [J]. Journal of Alloys and Compounds, 2019, 795: 314−318.

[59] WANG Xin, SHAO Yang, GONG Pan, YAO Ke-fu. The effect of simulated thermal cycling on thermal and mechanical stability of a Ti-based bulk metallic glass [J]. Journal of Alloys and Compounds, 2013, 575: 449−454.

[60] GUO Wei, SAIDA Jun-ji, ZHAO Mi, LÜ Shu-lin, WU Shu-sen. Thermal rejuvenation of an Mg-based metallic glass [J]. Metallurgical and Materials Transactions A, 2019, 50: 1125−1129.

[61] LUO Yu-sha, WANG Zhong, QIAO Jun-wei. Flow serrations of rejuvenation behaviour through cryogenic thermal cycling for Zr-based bulk metallic glass [J]. Philosophical Magazine, 2021, 101: 2261−2272.

[62] MENG Fang-qiang, TSUCHIYA K, KRAMER M J, OTT R T. Reduction of shear localization through structural rejuvenation in Zr−Cu−Al bulk metallic glass [J]. Materials Science and Engineering A, 2019, 765: 138304.

[63] MEYLAN C M, PAPPAROTTO F, NACHUM S, ORAVA J, MIGLIERINI M, BASYKH V, FERENC J, KULIK T,

GREER A L. Stimulation of shear-transformation zones in metallic glasses by cryogenic thermal cycling [J]. Journal of Non-Crystalline Solids, 2020, 548: 120299.

[64] HARUYAMA O, NAKAYAMA Y, WADA R, TOKUNAGA H, OKADA J, ISHIKAWA T, YOKOYAMA Y. Volume and enthalpy relaxation in $Zr_{55}Cu_{30}Ni_5Al_{10}$ bulk metallic glass [J]. Acta Materialia, 2010, 58: 1829−1836.

[65] LI Ning, LIU Lin, CHEN Qi, PAN Jie, CHAN K C. The effect of free volume on the deformation behaviour of a Zr-based metallic glass under nanoindentation [J]. Journal of Physics D: Applied Physics, 2007, 40: 6055−6059.

[66] WANG Xiao-dong, JIANG Jian-zhong, YI S. Reversible structural relaxation and crystallization of $Zr_{62}Al_8Ni_{13}Cu_{17}$ bulk metallic glass [J]. Journal of Non-Crystalline Solids, 2007, 353: 4157−4161.

[67] HARUYAMA O, INOUE A. Free volume kinetics during sub-T_g structural relaxation of a bulk $Pd_{40}Ni_{40}P_{20}$ metallic glass [J]. Applied Physics Letters, 2006, 88: 131906.

[68] HUO Li-shan, ZENG Ji-fang WANG Wei-hua, LIU C T, YANG Yong. The dependence of shear modulus on dynamic relaxation and evolution of local structural heterogeneity in a metallic glass [J]. Acta Materialia, 2013, 61: 4329−4338.

[69] SAMAVATIAN M, GHOLAMIPOUR R, ALI AMADEH A, MIRDAMADI S. Role of tensile elastostatic loading on atomic structure and mechanical properties of $Zr_{55}Cu_{30}Ni_5Al_{10}$ bulk metallic glass [J]. Materials Science and Engineering A, 2019, 753: 218−223.

[70] SAMAVATIAN M, GHOLAMIPOUR R, ALI AMADEH A, MIRDAMADI S. Extra rejuvenation of $Zr_{55}Cu_{30}Al_{10}Ni_5$ bulk metallic glass using elastostatic loading and cryothermal treatment interaction [J]. Journal of Non-Crystalline Solids, 2019, 506: 39−45.

[71] DU Yin, HAN Wei-chao, ZHOU Qing, XU Yu-hao, ZHAI Hai-min, BHARDWAJ V, WANG Hai-feng. Enhancing the plasticity of a Ti-based bulk metallic glass composite by cryogenic cycling treatments [J]. Journal of Alloys and Compounds, 2020, 835: 155247.

[72] DING Gan, JIANG Feng, SONG Xuan, DAI Lan-hong, JIANG Min-qiang. Unraveling the threshold stress of structural rejuvenation of metallic glasses via thermo-mechanical creep [J]. Science China: Physics Mechanics & Astronomy, 2022, 65: 264613.

[73] RI M C, SOHRABI S, DING Da-wei, DONG Bang-shao, ZHOU Shao-xiong, WANG Wei-hua. Serrated magnetic properties in metallic glass by thermal cycle [J]. Chinese Physics B, 2017, 26: 066101.

[74] RI M C, DING Da-wei, SUN Yu-hang, WANG Wei-hua. Microstructure change in Fe-based metallic glass and nanocrystalline alloy induced by liquid nitrogen treatment [J]. Journal of Materials Science & Technology, 2021, 69: 1−6.

深冷循环处理对金属玻璃结构和性能的影响

王明梓[1]，郭 威[1,2,3]，吕书林[1]，吴树森[1]

1. 华中科技大学 材料科学与工程学院 材料成形与模具技术国家重点实验室，武汉 430074；
2. 湖南大学 汽车车身先进设计与制造国家重点实验室，长沙 410082；
3. 华中科技大学 深圳研究院，深圳 518057

摘 要：近期研究表明，金属玻璃可通过热激励或机械激励的方法回春到更加亚稳的高能量状态，同时伴随着原子堆垛的松散化。回春过程可有效提高金属玻璃的宏观塑性。从金属玻璃弛豫与回春概念入手，简要介绍金属玻璃的回春手段，总结不同方法的优缺点。重点介绍深冷循环热处理(一种对样品形态无破坏性且适用性较高的回春方法)的效果、热处理参数对回春程度的影响以及回春后金属玻璃力学和磁性能的演化规律。最后，就金属玻璃回春行为进行分析，并对未来重要研究方向提出展望。

关键词：金属玻璃；回春；深冷循环；弛豫焓；塑性

(Edited by Bing YANG)